Int. J. Electrochem. Sci., 14 **(2019)** 7423 – 7436, doi: 10.20964/2019.08.33

International Journal of
ELECTROCHEMICAL
SCIENCE
www.electrochemsci.org

Corrosion Behavior of A356/SiC Alloy Matrix Composites in 3.5% NaCl Solution

Ociel Rodríguez Pérez[1,], J. A. García-Hinojosa[1], F. J. Rodríguez Gómez[1], S. Mejia-Sintillo[2], V.M. Salinas-Bravo[4], R. Lopes-Sesenez[2], J.G. Gonzalez-Rodriguez[2*], Cesar A. Garcia-Pérez[3].*

[1] Departamento de Ingeniería Metalúrgica, Facultad de Química, Universidad Nacional Autónoma de México, Circuito Exterior, Ciudad Universitaria, 04510, Ciudad de México, México.
[2] Centro de Investigación en Ingeniería y Ciencias Aplicadas-IICBA, Universidad Autónoma del Estado de Morelos, Av. Universidad 1001, Col. Chamilpa, 62210, Cuernavaca, Morelos, México.
[3] Tecnológico de Monterrey, Escuela de Ingeniería y Ciencias, Ave. Eugenio Garza Sada 2501, Monterrey, N.L., México, 64849.
[4] Instituto Nacional de Electricidad y Energías Renovables, Departamento de Combustión, Interior Internado Palmira, Cuernavaca, Mor., México.
[*]E-mail: ggonzalez@uaem.mx

Received: 2 April 2019 / *Accepted:* 21 May 2019 / *Published:* 30 June 2019

The corrosion behavior of the A356 (0, 5, 10, and 15 wt.%) SiC composites produced by mechanical alloying (MA) and uniaxially pressing/sintering route was studied through electrochemical and surface analysis techniques in 3.5 wt.% NaCl. The corrosion behavior of the samples was investigated by using electrochemical techniques. The corrosion resistance for the unreinforced A356 aluminum alloy was higher than the composites, however, when the A356 aluminum alloy was reinforced with SiC particles, composites were susceptible to a localized type of corrosion at the matrix/SiC particles interface. This made that although the passive zone for composites was wider with a pitting potential value slightly higher than those for base alloy, passivation current density was higher.

Keywords: A356/SiC composites, mechanical alloying, electrochemical techniques.

1. INTRODUCTION

A356 aluminum alloy has been attractive to their physical and chemical properties including low density, moldability, good weldability, high corrosion resistance, as well as a moderate strength, and good ductility. A356 aluminum alloy is used for structural applications in aircraft, automobile, and military industries [1-4]. It can also be used as a substitute for aluminum alloy 6061. Due to their high specific strength, lightweight, good wear and corrosion resistance, A356 aluminum alloy has been reinforced with ceramics turning into aluminum matrix composites (AMCs) that are being used in

widespread applications [5, 6]. In order to fabricate AMCs, many reinforcements such as SiC, Al_2O_3, TiC, ashes, graphite, etc. have been used by different authors [7-10]. Silicon carbide (SiC) is one of the most widely used dispersoids in AMCs. This high interest is due to its high melting point, high stiffness (480 GPa), good thermal stability, high hardness, low price, provides the compound with high strength and elastic modulus [11, 12].

However, due to the fact that corrosion resistance is imparted by a protective oxide film (Al_2O_3) on the surface, one of the main disadvantages of particulate reinforced aluminum matrix composites (AMCs) is the influence of reinforcement on the corrosion resistance. This protective filmT can present discontinuities or flaws due to the addition of a reinforcing phase, which can increase the sites for corrosion initiation and rendering the composite liable to severe corrosion attack [13] or to be obstacles for the formation of the passive film. If the oxide layer will break, aluminum alloy itself recovers and generate a thin layer of the oxide film on the surface.

In addition to this, their corrosion behavior can be affected by the manufacturing processes like stir cast, mechanical alloying, powder metallurgy, in situ or squeeze cast. Among the variety of manufacturing processes, mechanical alloying (MA) is an important technique for preparation of AMCs, the most important advantage of MA is the feasibility of addition of alloying elements in order to improve mechanical and physical properties of metallic alloys. MA over melting route is considered as a promising and commercial technique because it ensures a homogeneous distribution of both, the alloying elements and the reinforcement materials without the segregation phenomena typical of the casting processes, or the agglomeration of the submicron reinforcing particles and poor adhesion [14, 15].

The determination of the corrosion behavior of composite materials reinforced with ceramic additives is very important. Researches about AMCs have been focused on the corrosion susceptibility in NaCl solutions [16, 17]. Trzaskoma and McCafferty [18] evaluated the corrosion behavior of SiC/Al2024, SiC/Al6061 and SiC/Al5456 composites fabricated by powder metallurgical route in 0.1N and 0.8N NaCl by using polarization curves. They found that the polarization curves and pitting potential values of composites and their respective matrix alloys were very similar except Al2024 system. In another research work [19] the effect of C, Al_2O_3 or SiC on the corrosion behavior of Al 6061 based MMCs were investigated [19]. The pitting potentials of matrix and its composite containing SiC were similar, with the initiation of a pit was greater in the composite than in the matrix due to the galvanic coupling of carbon fibers and aluminum. They also found a beneficial effect on the stress corrosion cracking resistance for the MMC by ageing of Al 7075/SiC composite at 170° C for more than 1 h following at 110°C in 3.5 % NaCl which included an increase in the pitting potential also. The susceptibility to pitting corrosion of a mechanically alloyed MMC based on Al1050 with the addition of 20 wt. % of different size (3 and 20 μm) in 1N NaCl at 25 °C was carried out [20]. This procedure left voids at the reinforcement/matrix interface causing an increase in the pitting attack with the addition of SiC. As it can be seen, the corrosion behavior of A356/SiC composites produced by mechanical alloying technique has not widely reported by researchers, only their mechanical properties have been extensively studied. Thus, the aim of this study was to investigate the corrosion behavior of A356 (0, 5, 10, and 15 wt.%) SiC composites produced by mechanical alloying (MA) and uniaxially pressing/sintering route. The output from this research will be helpful in understanding the corrosion of these peculiar AMCs.

2. EXPERIMENTAL PROCEDURE

2.1. Synthesis of the composites

In this study, A356 powders obtained by powder metallurgy technique from the A356 aluminum alloy ingot (density of 2.686 g/cm^3, <60 Mesh) were used as the matrix powders. Silicon carbide particles (density of 3.22 g/cm^3, an average particle size of 38 μm, Aldrich, 97.5 %) were used as the reinforcement into the aluminum matrix to produce composites by the MA technique. Chemical composition of A356 aluminum alloy ingot used in this study is shown in Table 1.

Table 1. The chemical composition of A356 aluminum alloy (wt. %).

Al	Si	Fe	Cu	Mn	Mg	Zn	Ti	Sr
Balance	7.26	0.36	0.01	0.012	0.31	0.02	0.013	.0002

The percentages of SiC particles (wt.%) were 0, 5, 10 and 15 and the milling time was 10 h. The experimental procedure consisted of the mixture of A356 powders and silicon carbide particles (0, 5, 10, and 15 wt.% SiC) using a planetary high energy ball mill (Fritsch–P7). The powders mixtures were milled during 10 h at 280 rpm under argon atmosphere. Ethanol (2 ml) was used as a process control agent (PCA) to prevent excessive cold welding during milling of the powders particles. The size of the stainless steel balls used for the milling was (10 mm and 12 mm diameters), the mass of the powders was of 10 g, and the ball to powder weight ratio (BPR) was 5:1. The as-milled powders obtained by MA were uniaxially cold pressed in cylindrical steel die at 400 MPa in order to obtain samples with 10 mm of diameter and 5 mm high. Green products were sintered at 500 ˚C during 5 h under an argon atmosphere. X-ray diffraction of specimens was carried out in a D2 PHASER diffractometer. Microscopic characterization of specimens was carried out by using a scanning electronic microscope (SEM) JEOL JSM-5900LV (15kV) attached with energy dispersive X-ray (EDX). For this, specimens were mounted in a polymeric resin, prepared by grinding on SiC metallographic paper from 240 to 1000-grit, polished with alumina (0.5 μm) followed by successively cleaning in ethanol and then distilled water using an ultrasonic bath for 15 min.

2.2. Corrosion tests

The corrosion evaluation was performed by using electrochemical techniques including potentiodynamic polarization curves, electrochemical impedance spectroscopy (EIS) and linear polarization resistance measurements (LPR). Electrochemical measurements were conducted in a three-electrode glass cell using a Gamry PC4 300 potentiostat controlled by Gamry Instruments Framework software. The working electrodes were encapsulated in commercial epoxy resin, prior to the preparation described in section 2.1, leaving unmasked a circular area of 0.5 cm^2. A graphite rod with an immersed area of 4 cm^2 and a saturated calomel electrode (SCE) were used as auxiliary and reference electrode, respectively. The experiments were done at room temperature with the solution open to the air. All tests

were conducted using freshly prepared test specimens and were repeated three times to ensure the accuracy and the reproducibility of the data. The specimens were allowed to stabilize at open circuit potential (OCP) for 30 min prior to the electrochemical tests. EIS measurements were carried out, at 0 V vs. OCP, AC voltage 10 mV rms, frequency range 10 kHz to 0.04 Hz with 10 points/decade. Potentiodynamic polarization tests were carried out by polarizing the specimen from -1000 up to +1000 mV vs. OCP, voltage 1 mV/s. LPR tests were carried out by polarizing the specimens from -10 to +10 mV with respect the OCP value at a scan rate of 1 mV/s during 24 hours. Corroded surfaces of composites samples were established by scanning electronic microscope (SEM) JCM-6000Plus with and energy dispersive X-ray analyzer (EDX) attached to it.

3. RESULTS AND DISCUSSION

3.1. Composites characterization

The X-ray diffraction analysis (XRD) for the consolidated samples is given in Fig. 1. As shown in this figure, the XRD patterns not only show the characteristic peaks of aluminum and silicon, but also the ones belonging to the silicon carbide particles, excluding the unreinforced A356 aluminum alloy which was produced as a reference specimen. The absence of additional peaks indicates that no unwanted phases have been formed in detectable quantities during mechanical alloy. The intensity of the SiC (111) peak of the consolidated samples increased with the increasing weight fraction of SiC particles in the composite whereas the Al (111) peak became less broad. The average of crystallite sizes (D) of the consolidated samples were calculated using the full peak width at half maximum (FWHM) of Al (111), Al (200), Al (220) and Al (311) peaks of the XRD patterns. The crystallite size values for the consolidated samples with 0, 5, 10, and 15 wt.% SiC is 41, 40, 42, and 37 nm, respectively.

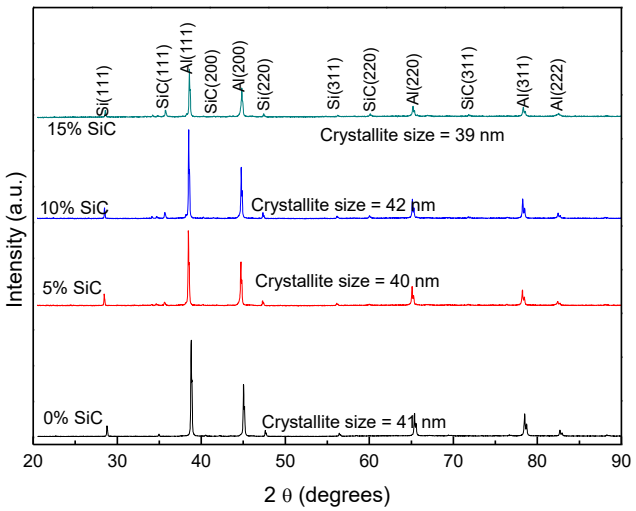

Figure 1. X-ray diffraction patterns of the different A356/SiC composites.

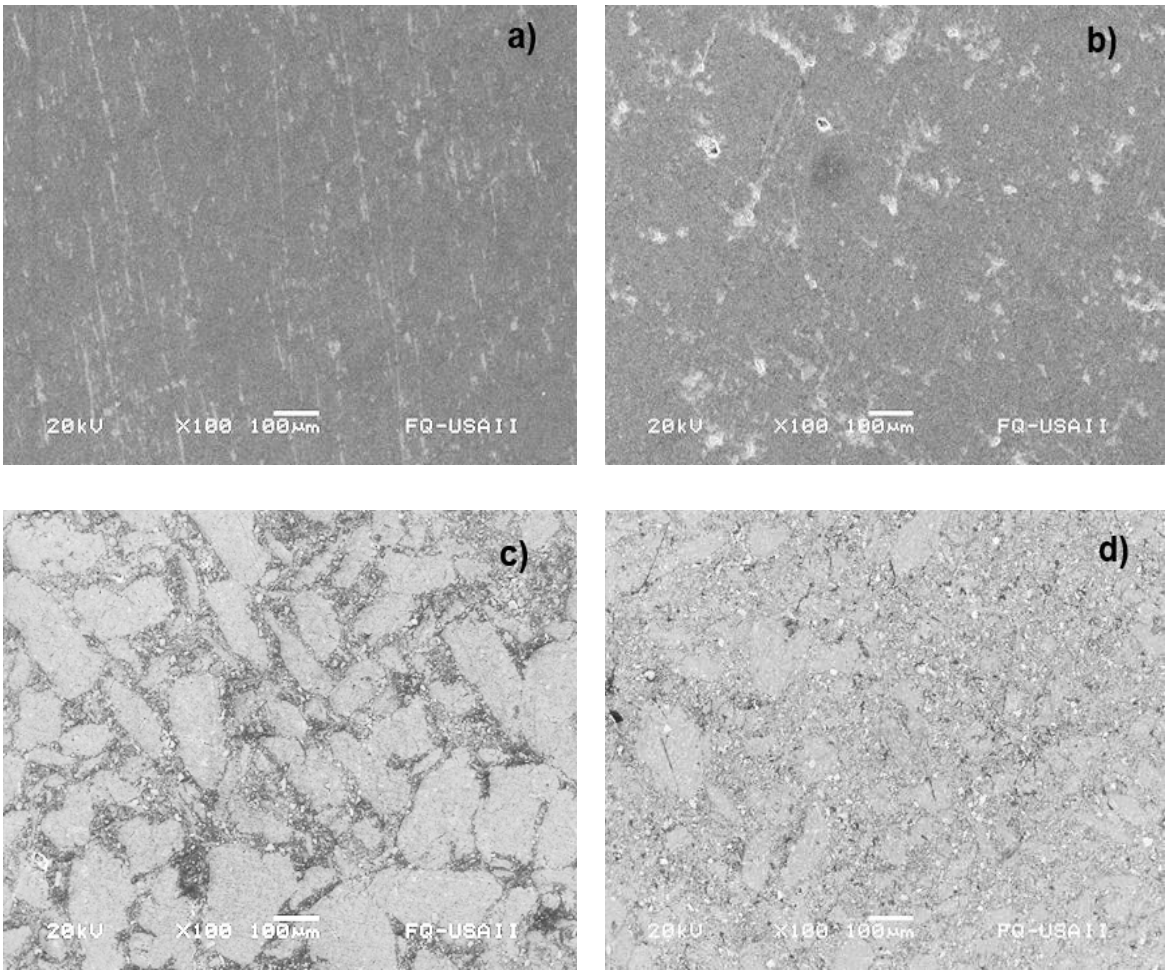

Figure 2. SEM micrographs showing the microstructures of the different A356/SiC composites containing a) 0, b) 5, c) 10, and d) 15 wt.% SiC.

On the other hand, micrographs of specimens containing different SiC contents are shown in Fig. 2. The microstructure shows the presence of porosity associated as a result of cold pressing and temperature of sintering. Also, this figure shows that by increasing the amount of SiC leads to the presence of finer grain in the samples. During the sintering step, the hardness of the SiC has impeded grain growth giving as a result the reduction in grain size and thus an improvement in the hardness of the consolidated samples. The number of grain boundaries is maximized by the reduction in the grain size, improving the mechanical properties.

3.2. Electrochemical tests

The effect of SiC contents on the A356 base alloy on the open circuit potential value, OCP, is given in Fig. 3. It can be seen that the addition of reinforcement SiC particles brings a shift in the OCP value towards more active values as compared to that value for the base alloy, which indicates a higher thermodynamic trend to higher corrosion rates for the composites. This behavior has been reported by other researchers, for instance in [21], where the corrosion behavior of Al–Mg–Si alloy matrix hybrid

composites reinforced with rice husk ash and silicon carbide in 3.5 NaCl solution. However, there was not a clear trend of the OCP value with the SiC particulates contents, since the most active OCP value was for the lowest SiC contents, i.e 5%, but the detrimental effect of the silicon carbide particulates addition on the corrosion behavior is clear.

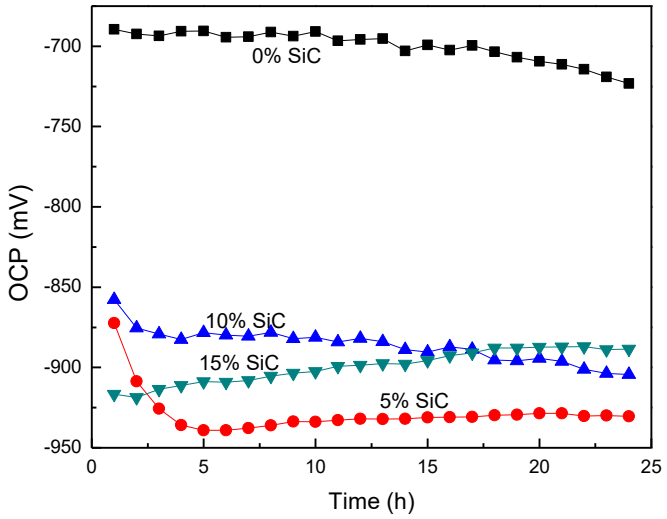

Figure 3. Change on the OCP value with time for the different A356/SiC composites tested in 3.5% NaCl solution.

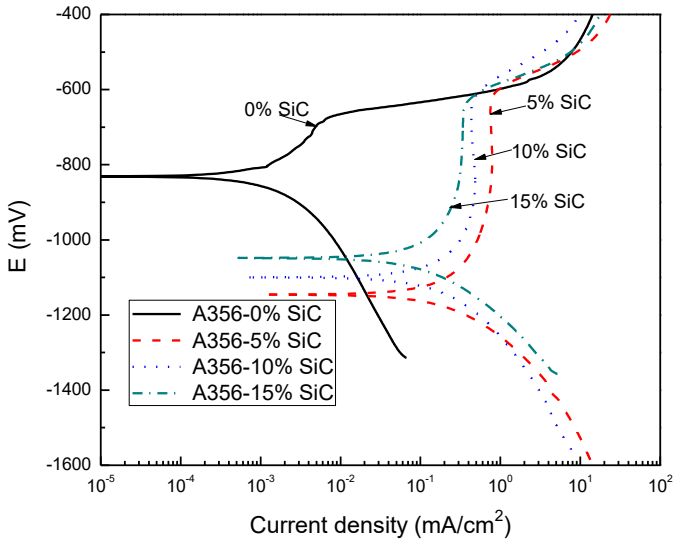

Figure 4. Effect of the SiC contents on the polarization curves for the different A356/SiC composites tested in 3.5% NaCl solution.

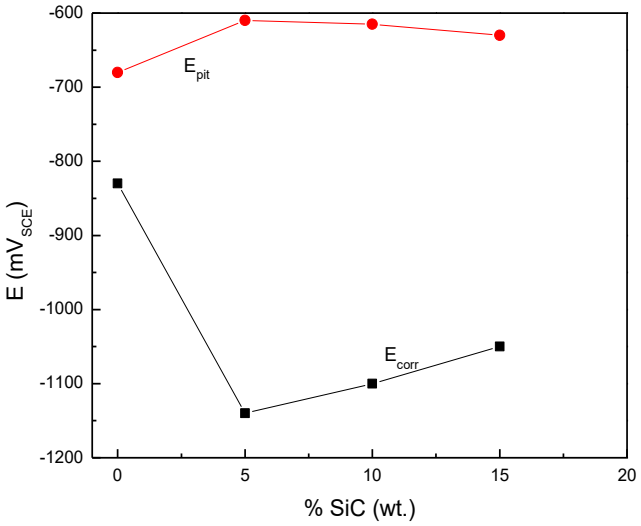

Figure 5. Effect of the SiC contents on the E_{pit} and E_{corr} values for the different A356/SiC composites tested in 3.5% NaCl solution.

The effect of SiC contents on the polarization curves for the different A356/SiC composites is given in Fig. 4. All the materials displayed an active-passive behavior due to the formation of an Al_2O_3 layer, however, for the base A356 aluminum alloy, the E_{corr} value was the noblest, whereas they were more active for the composites, just as the obtained values in Fig. 3. The passive zone for the base alloy was from a potential value slightly more anodic than -800 mV and it ended where a pitting potential value, E_{pit}, was reached, i.e. -690 mV.

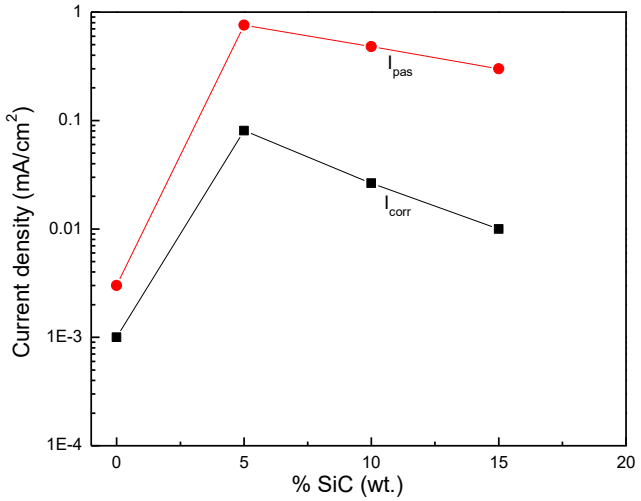

Figure 6. Effect of the SiC contents on the I_{pas} and I_{corr} values for the different A356/SiC composites tested in 3.5% NaCl solution.

Instead, the composites had a much wider passive zone, since the E_{corr} value was shifted towards more active values, between 200 and 300 mV more negative than that for base alloy, and the E_{pit} value was marginally shifted towards more anodic values, for around 50 mV, as it can be seen in Fig. 5. However, despite the fact that the passive zone was much wider for the composites than that for the A356 aluminum alloy, the I_{corr} and passive current density values, I_{pas}, were higher for the composites than those for the base alloy, as shown in Fig. 6.

This can be due to the fact that the presence of SiC particulates are sites for the disruption of the passive layer, and that they act as cathodic zones as compared with the matrix, which acts as anodes and, thus, leading to a galvanic attack. Although the passive layer can be disrupted by these particles, once they are exposed to the electrolyte, they are detached from the surface and washed away, the accumulation of corrosion products leads to the formation of the passive layer once again. However, on the sites where the SiC particles were detached, localized type of corrosion such as pits can occur. Similar results were obtained by Pinto et al. [13] as well by Pardo et al. [22]. They argued that the for the localized corrosion commonly observed in MMCs is caused by the presence of heterogeneities such as grain boundary, intermetallic, reinforcement/matrix interface, inclusion, defect, etc. [23, 24]. A difference in the electrochemical potential between these defects and the matrix causes the matrix to act as anode and to be corroded [25]. In our case, we have seen that the grain size decreased with an increase in the SiC contents, the reduction in the grain size maximizes the number of grain boundaries, causing more paths for the corrosion process to take place.

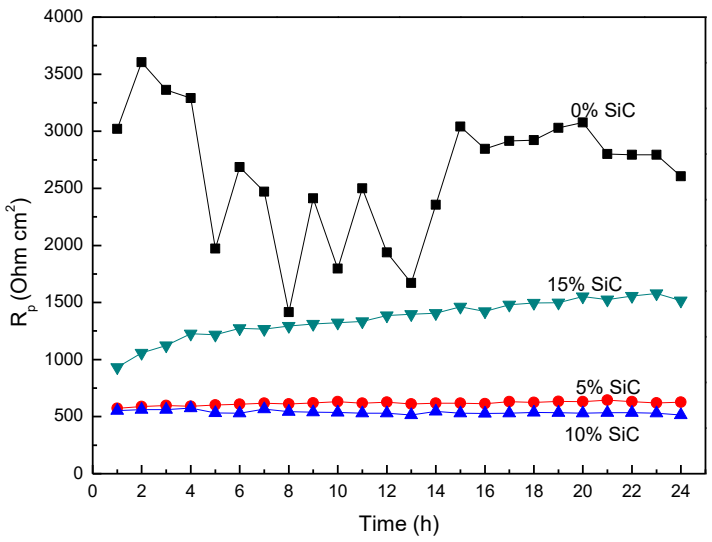

Figure 7. Change on the R_p value with time for the different A356/SiC composites tested in 3.5% NaCl solution.

The change on the R_p value with time for the different composites is given in Fig. 7. It can be seen from this figure, that the highest R_p value was exhibited by the A356 base aluminum alloy, whereas the composites had lower R_p values, where the composite having 15% SiC exhibited an intermediate R_p

value. Since the I_{corr} value is inversely proportional to the R_p value through the Stern-Geary equation, from Fig. 7 we can say that A356 base aluminum alloy had a higher corrosion resistance than the different composites, just as shown by the polarization curves. Due to the formation of micro galvanic cells between the matrix and the reinforcements, MMCs are generally susceptible to corrosion, causing a selective corrosion at the interface, where tha matrix generally behaves as [26]. Thus, as compared to their respective metallic matrix, MMC are more susceptible to corrosion due to reinforcement phase which causes brake down of protecting film. The presence of Cl^- in the solution will cause a Brake down of film. In this way, rather improving the corrosion resistance, the reinforcement phase is an obstacle for protecting passive film, which is the responsible for the corrosion resistance of the Al matrix. In the matrix Al alloy generate this passive film recovering itself if it is destroyed, which does not occur in a MMCs since the reinforcement avoids this film to be reformed, allowing pitting and crevice corrosion of underlying substrate. By increasing the number of reinforcement particles the number of sites where the film presents discontinuities increases increasing the sites for corrosion initiation.

EIS data in both Nyquist and Bode formats for the different A356 base aluminum composites are given in Fig. 8. Nyquist diagrams display one capacitive loop at high and intermediate frequencies, followed by straight-line at lower frequencies. This behavior is a typical of an Al-base alloy undergoing localized type of corrosion [27, 28] due to localized galvanic attack of the more active matrix by the nobler SiC particle.

The high and intermediate frequency loop which is attributed to the general corrosion of the metal, with the formation of the passive layer, whereas straight-line is due to the diffusional process that occurs inside the pits. Bode diagrams in the impedance format indicates that the highest impedance value corresponds for the base Al-base alloy for more than one order of magnitude, and this is decreased for the composites.

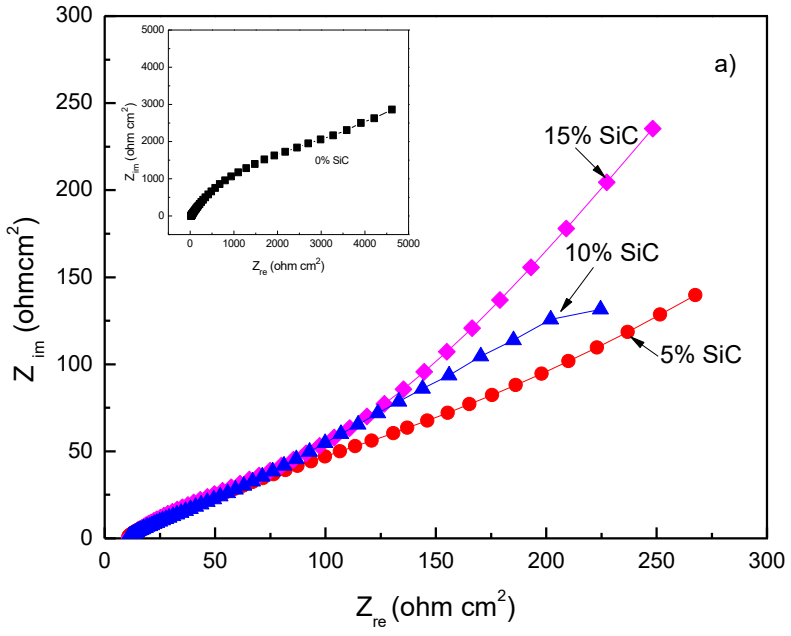

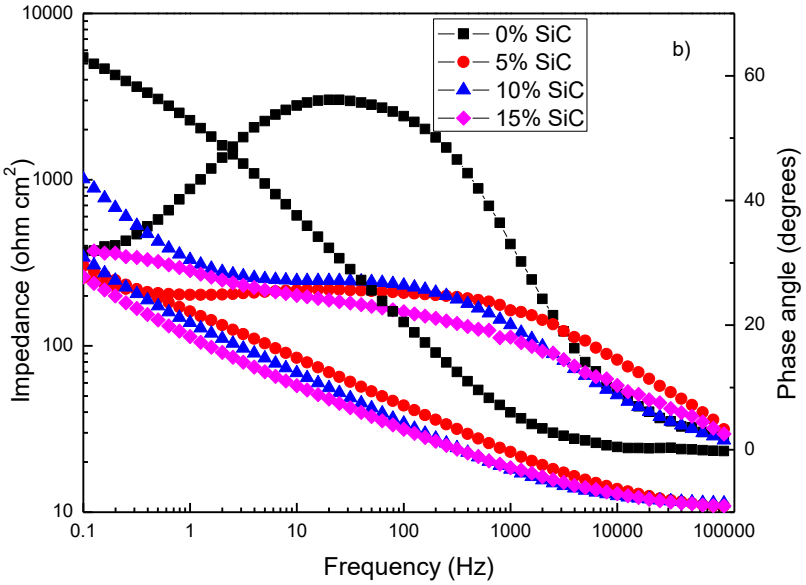

Figure 8. Effect of the SiC contents in the a) Nyquist and b) Bode plots for the different A356/SiC composites tested in 3.5% NaCl solution.

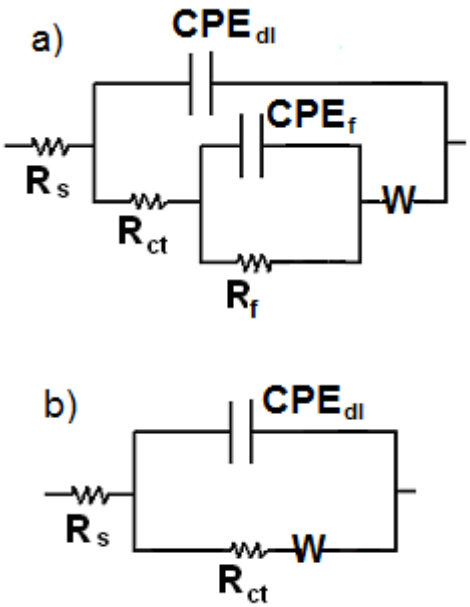

Figure 9. Electric circuits used to simulate the EIS data for a) A356 alloy and b) A356/SiC composites.

The plot of the log (impedance) versus the log (frequency) shows the existence of two slopes for the Al-base alloy and only one for the composites, and thus two time constants for the base alloy and only one for composites. The phase angle is maximum for the Al-base alloy and it decreases rapidly for the composites; in addition to this, the maximum phase angle remains constant over a wide frequency

interval for the base alloy, indicating the existence of two time constants, whereas for the composites this was not so evident.

The impedance behavior of the different composites can be described by equivalent circuits shown in Fig. 9. In these circuits, R_s corresponds to the solution resistance, CPE_{dl} and R_{ct} are the double electrochemical layer capacitive behavior and charge transfer resistance, CPE_f and R_f are the capacitive behavior of the corrosion products film and its resistance, whereas W is the Warburg diffusion element and R_w the diffusion layer resistance. CPE was used to describe non-ideal capacitive behavior of heterogeneous interface. The impedance of a CPE is described as:

$$Z_{CPE} = \frac{1}{Y_0(j\omega)^n} \quad (1)$$

where Y_0 is the magnitude of the CPE, j is the imaginary unit, ω is the angular frequency ($\omega = 2\pi f$, where f is the AC frequency), and n is the CPE exponent (phase shift) [29] which provides some surface parameters such as roughness. Obtained parameters by using circuits shown in Fig. 9 are given in table 2.

Table 2. Obtained parameters from the simulation of the EIS data for Al-base composites.

%SiC	CPE_{dl} ($\mu Ss^n/cm^2$)	n	R_{ct} (ohm cm^2)	CPE_{dl} ($\mu Ss^n/cm^2$)	n	R_f (ohm cm^2)	R_w (ohm cm^2)	n
0	8.4×10^{-5}	0.7	4.9×10^{3}	3.5×10^{-4}	0.9	5.0×10^{3}	2.4×10^{-2}	0.9
5	2.2×10^{-3}	0.4	1.4×10^{2}	--	--	--	1.8×10^{-2}	0.5
10	1.3×10^{-3}	0.5	4.2×10^{2}	--	--	--	2.3×10^{-1}	0.6
15	3.6×10^{-3}	0.4	7.0×10^{2}	--	--	--	8.1×10^{1}	0.3

3.3. Surface characterization

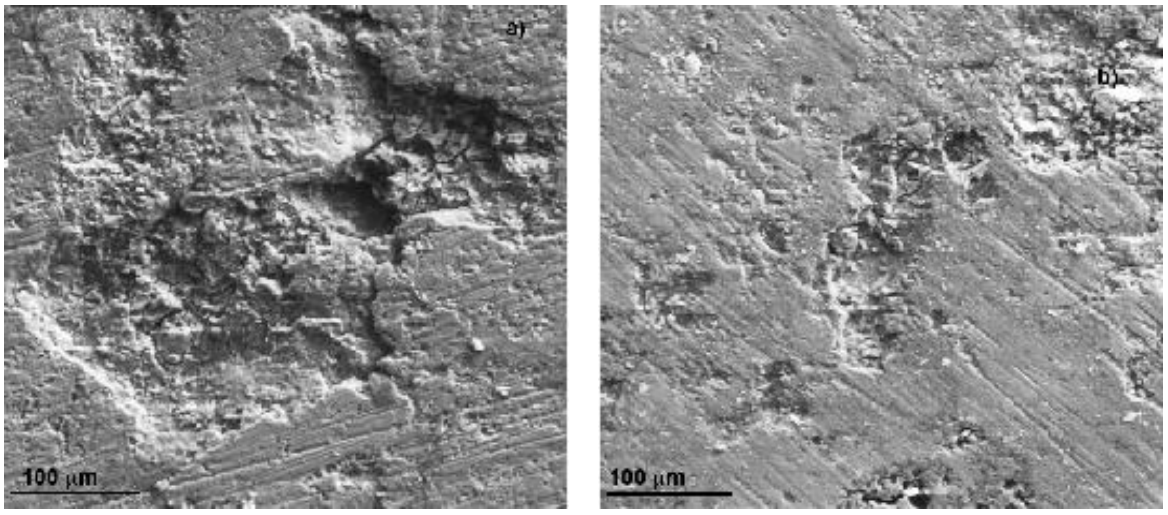

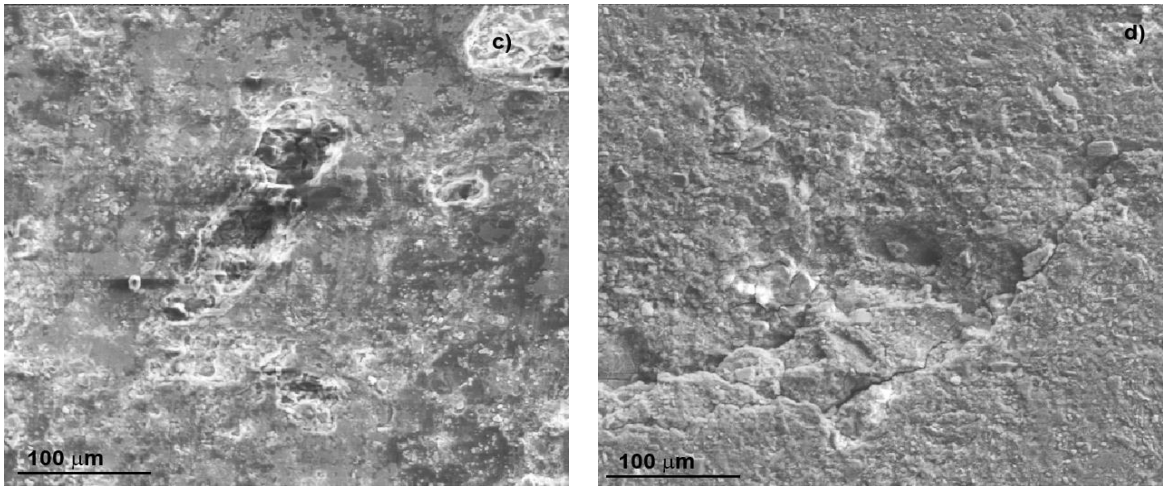

Figure 10. SEM micrographs showing the corroded surfaces of the different A356/SiC composites containing a) 0, b) 5, c) 10, and d) 15 wt.% SiC corroded in 3.5% NaCl solution.

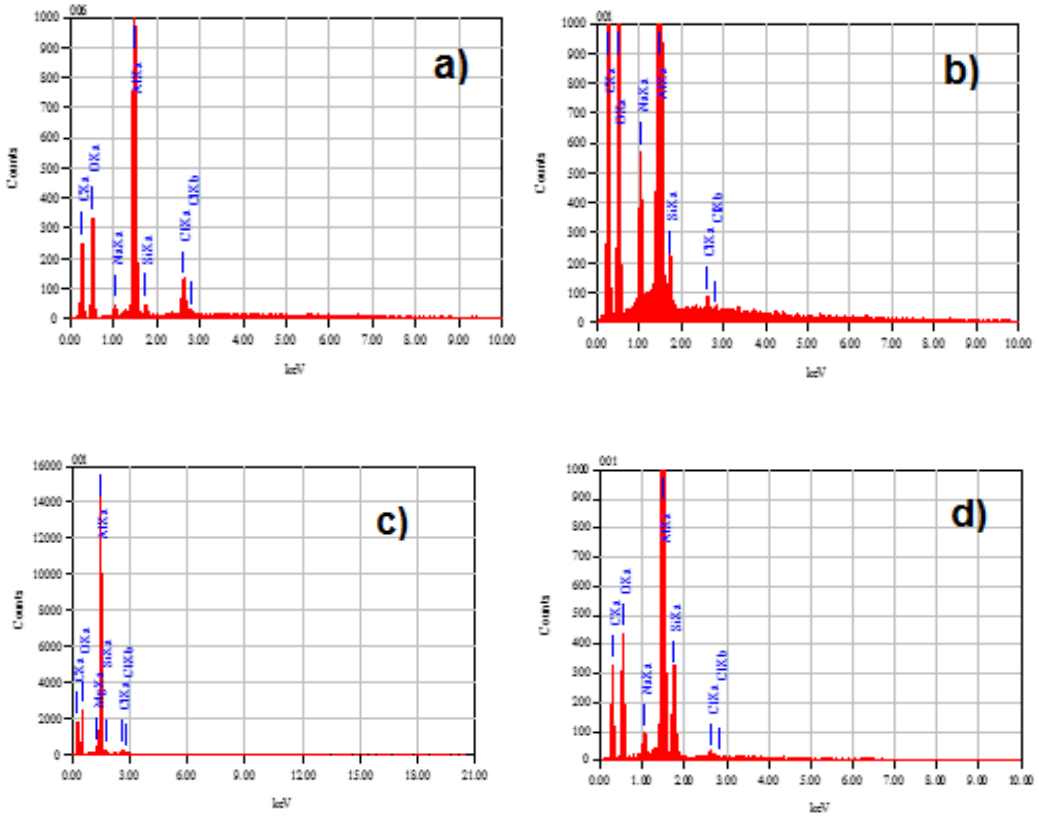

Figure 11. EDX analysis the corroded surfaces of the different A356/SiC composites containing a) 0, b) 5, c) 10, and d) 15 wt.% SiC corroded in 3.5% NaCl solution.

For Al356 alloy, the charge transfer and passive film resistance values were similar, indicating that both of them are responsible for the corrosion resistance of this alloy. The diffusion resistance value, which, as stated above, refers to the diffusion inside the pits, is much lower than the R_f and R_{ct}, indicating that for this material, localized type of corrosion dominates over the uniform corrosion. However the R_{ct}

value for the Al-base alloy is much higher than that for the composites, as expected, since the corrosion resistance of the later was lower than the former. The R_w value for the composites was much lower than that for R_{ct} especially for the alloy containing 5% SiC, indicating that in the later localized type of corrosion dominates over the uniform type of corrosion. The difference between the R_w and R_{ct} values for the composites containing 10 and 15% SiC, indicating that probably for these alloys localized type of corrosion did not dominate over the uniform type of corrosion.

Micrographs of corroded specimens shown in Fig. 10 indicates that Al356 alloy and composite containing 5% SiC exhibited shallow pits on their surface, whereas composites containing either 10 or 15% SiC exhibited predominantly of uniform type of corrosion. EDX analysis of the corrosion products layers formed on the different composites are shown in Fig. 11, which shows the presence of Al, Si, C, O and Na as the main chemical elements, suggesting the formation of Al_2O_3. A summary of this chemical analysis is given in table 3, which indicates that the contents of Al is the lowest in the Al-base alloy due to the lowest corrosion rate that this alloy exhibited.

Table 3. Semi quantitative chemical analysis (at. %) done to the corrosion products layer formed on top of the different Al-base composites corroded in 3.5% NaCl solution.

%SiC	Al	Si	C	O	Na
0	**12.2**	**0.4**	**53**	**32.1**	**0.4**
5	**18.6**	**0.4**	**53**	**27**	**0.4**
10	**17.6**	**3.0**	**52.1**	**26.2**	**0.8**
15	**15.5**	**0.5**	**51.7**	**30.4**	**1.7**

On the other hand, the amount of Al was the highest for the composite containing 5% SiC probably due to the fact that this specimen exhibited the highest corrosion rate and the thickest layer of corrosion products was built up on its surface.

4. CONCLUSIONS

The corrosion behavior of A356 (0, 5, 10, and 15 wt.%) SiC composites has been examined in 3.5% NaCl by using electrochemical methods, the following conclusions are made. Polarization curves showed that composites exhibited a wider passive zone and a higher pitting potential value than those for A356 alloy, however they showed a higher passive current density value. Corrosion rate of A356 alloy was higher than that for composites, especially for the one containing 5% SiC. Corrosion process was given by the formation of a passive layer, however, this was disrupted at the matrix/SiC interface, giving rise to localized type of corrosion such as pitting which was more evident for the composite containing 5% SiC. For composites containing either 10 or 15% SiC uniform type of corrosion was the main type of attack.

ACKNOWLEDGEMENTS
Ociel Rodriguez Pérez is thankful for the postdoctoral fellowship DGAPA-UNAM. Also, He would like to thank the Department of Metallurgical Engineering of the Faculty of Chemistry, UNAM for the facilities provided for the development of this project.

References

1. B. Prabhu, C. Suryanarayana, L. A., R. Vaidyanathan, *Mater. Sci. Eng. A*, 425 (2006) 192.
2. J. Milligan, R. Vintila, M. Brochu, *Mater. Sci. Eng. A*, 508 (2009) 43.
3. N. Kang, P. Coddet, H. Liao, T. Baur, C. Coddet, *Appl. Surf. Sci*., 378 (2016) 142.
4. N. Chawla and K. K. Chawla, Metal Matrix Composites, Springer Science and Business Media, Inc., (2006) NY., USA.
5. G. B. V. Kumar, C. S. P. Rao, N. Selvaraj, M. S. Bhagyashekar, *J. Minerals and Materials Characterization and Engineering,* 9 (2010) 43.
6. J. Safari, G. H. Akbari, A. Shahbazkhan, M. D. Chermahini, *J. Alloys Compd*., 509 (2011) 9419.
7. X. Yao, Y. F. Zheng, J. M. Liang, D. L. Zhang, *Mater. Sci. Eng. A*, 648 (2015) 225.
8. A. Javdani, V. Pouyafar, A. Ameli, A. A. Volinsky, *Mater. Desig.*, 109 (2016) 57.
9. S. D. Saravanan, M. S. Kumar, *Procedia Eng*., 64 (2013) 1505.
10. M. Cabeza, I. Feijoo, P. Merino, G. Pena, M.C. Pérez, S. Cruz, P. Rey, *Powder Technol*., 321 (2017) 31.
11. E. C. Cesar., V. L. Francisco, T. C. Jose, *Rev. Metal*., 36 (2000) 179.
12. S. Valdez, J. Ascencio, S.R.Casolco, M.I.Pech-Canul, *Int. J. Electrochem. Sci*., 9 (2014) 6225.
13. G. M. Pinto, J. Nayak, A. N. Shett, *Int. J. Electrochem. Sci.,* 4 (2009) 1452.
14. J. B. Fogagnolo, M. H. Robert, E. M. Ruiz-Navas, J. M. Torralba, *J. Mater. Sci*., 39 (2004) 127.
15. J. Rui-Song, W. Wen-Hu, S. Guo-Dong, W. Zeng-Qiang, *J. Manuf. Process*., 23 (2016) 249.
16. M. K. Abbass, K. S. Hassan, A. S. Alwan, *Int. J. Materials, Mechanics and Manufacturing*, 3 (2015) 31.
17. H.M. Zakaria, Ain Shams, *Engineering Journal,* 5 (2014) 831.
18. P. P. Trzaskoma, E. McCafferty, *J. Electrochem. Soc.,* 130 (1983) 804.
19. Yoshiaki Shimizu, Toshiyasu Nishimura, Lwao Matsushima, *Mat.Sci. Eng. A*, 198 (1995) 113.
20. A.J. Trowsdale, B. Noble, S.J. Harris, I.S.R. Gibbins, G.E. Thompson, G.C. Wood, *Corros. Sci.,* 38 (1996) 177.
21. K. K. Alaneme, T. M. Adewale, P. A. Olubambi, *J. Mater. Res. Technol,*. 3 (2014) 9.
22. A. Pardo, M.C. Merino, S. Merino, F. Viejo, M. Carboneras, R. Arrabal, *Corros. Sci.,* 47 (2005) 1750.
23. K. K. Alaneme, *Leonardo J. Sci*., 18 (2011) 55.
24. P.D. Reena Kumari, J. Nayak, A. Nityananda Shetty, *Arabian J Chem.,* 9 (2016) S1144.
25. A. Onat, *J Alloys Compd*., 489 (2010) 119.
26. Hosni Ezuber, A. El-Houd, F. EI-Shawesh, *Materials and Design,* 29 (2008) 801.
27. K. Jafarzadeh, T. Shahrabi, M.G. Hosseini, *J. Mater. Sci. Technol.,* 24 (2008) 215.
28. M.C. Pardo, R. Merino, F. Arrabal, M. Carboneras, *J. Electrochem. Soc*., 153 (2006) B52.
29. F. B. Growcock, R. J. Jasinski, *J. Electrochem. Soc.,* 136 (1989) 2310.